Hindawi
Mathematical Problems in Engineering
Volume 2021, Article ID 1088805, 19 pages
https://doi.org/10.1155/2021/1088805

Research Article

Optimal Cooperative Brake Distribution Strategy for IWM Vehicle Accounting for Electric and Friction Braking Torques

Michele Vignati, Mattia Belloni, Davide Tarsitano, and Edoardo Sabbioni

Department of Mechanical Engineering, Politecnico di Milano, via La Masa 1, Milan 20156, Italy

Correspondence should be addressed to Michele Vignati; michele.vignati@polimi.it

Received 19 May 2021; Revised 24 June 2021; Accepted 29 June 2021; Published 10 July 2021

Academic Editor: Xiaodong Sun

Electric vehicles are spreading in automotive industry pushed by the need of reducing greenhouse gas. However, the use of multiple electric motors, i.e., one per wheel, allows to redefine the vehicle powertrain layout with great benefits on vehicle dynamics. Electric motors braking torque is in general not enough to produce high decelerations. Hydraulic friction brakes are still necessary for safety reasons and to avoid oversized motors. This paper presents a control strategy for distributed electric motors (EM), one per wheel, to maximize the regenerative braking. The controller handles cooperative braking among EMs and hydraulic brakes, which are still necessary to guarantee top braking performance of the car. The proposed algorithm considers the driver requested braking torque as well as the required yaw moment by stability control system. Motor efficiency map and wheel normal load are considered to optimally distribute the torques. With respect to conventional distribution strategies, the presented algorithm improves performance, maximizing the regenerative braking power.

1. Introduction

In recent years, the interest towards electric vehicles (EVs) leads to the possibility of reinventing several vehicle subsystems, for both light and heavy-duty vehicles [1], in particular the powertrain. The use of multiple electric motors (EMs), one per wheel, allows to precisely control the torque at each wheel showing superior performance with respect to a traditional internal combustion engine (ICE) vehicle [2]. In addition, EMs can deliver also braking torques, thus recovering some of the vehicle kinetic energy, i.e., regenerative braking used to recharge the vehicle battery [3]. In-Wheel Motors (IWM) are one smart solution [2] for having distributed electric motors (DEMs). Furthermore, the demand of extremely reliable motors and the cost reduction pushes the research to find innovative solution for controlling Permanent Magnets EMs with powerful sensorless solutions ([4–7]).

Another interesting feature offered by DEMs is the possibility of easily applying Torque Vectoring (TV) to improve the stability and performance of the car ([8–11]). Furthermore, antilock braking systems (ABS) can benefit from EMs higher promptness, even when compared to hydraulic actuated mechanical brakes, thus reducing the car stopping distance ([2, 3]). Despite the fact that DEMs solutions appearing in the market have extremely high performances considering the maximum delivered torque and power, the maximum braking torque is not enough to brake the car at high deceleration values. It is thus necessary to use conventional friction brakes in cooperation with DEMs, and a suitable blended braking control strategy must be adopted. Several parameters have to be accounted for when dealing with it like wheel peripheral speeds, motor efficiency, load transfers, battery Status of Charge (SOC), etc. Furthermore, the total braking torque required by driver and the yaw moment required by TV must be satisfied.

When dealing with DEM vehicles, considering the typical control layout ([8, 9, 11–13]) of vehicle dynamics control strategies inside Vehicle Control Unit (VCU) can be schematized as in Figure 1. The driver steer command inputs into vehicle with accelerator and brake pedal inputs are processed by VCU to generate total driving and braking torque to be demanded in electric motors. The VCU also generates a torque vectoring yaw moment to stabilize or

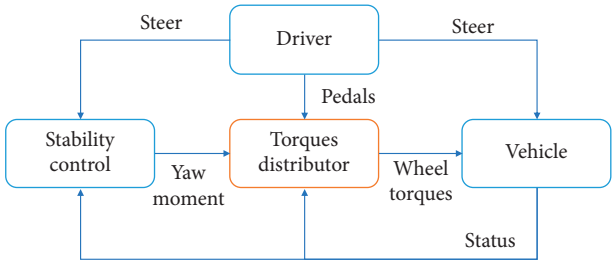

Figure 1: Typical scheme for electric vehicles with multiple electric motors.

improve the performance of the car. The total torque and total yaw moment must be distributed among the available motors and hydraulic brakes. This latter aspect is the focus of this paper.

The resulting problem is a constrained multi-input system. In literature, the problem is usually divided in three parts: front-rear axle brake repartition, electrical-mechanical brake repartition at each wheel, and electric power management.

In [14], a hybridized vehicle equipped with in-wheel motors has a braking logic based on a load transfer estimation control algorithm. On the vehicle with four in-wheel motors in [15], a deep learning optimization algorithm finds the braking repartition considering design variables as the front-rear brake repartition and the electrical-mechanical torque repartition at each axle. Authors of [16] propose to use the maximum brake torque available at the motor keeping in consideration the wheel peripheral velocity, available motor torque considering motor saturation, and the battery SOC. In [17], authors suggest using a fixed front-rear brake repartition that favors the braking on the front axle, using as much motor torque as the motor can provide (maximum motor torque limitation). Also, in [18], authors suggest using optimal front-rear repartition curve, but a fuzzy logic controller based on torque variation rate and battery SOC allocates mechanical and electrical torque at each wheel. An optimal control strategy is proposed by Xu et al. [12]; it is based on MPC that minimizes a cost functional that involves the optimal front-rear force repartition, the driver torque demand, the EM efficiency, and the efficiency of the brake system. Paper [19] proposes an electronically controlled braking system for EV and HEV, which integrates regenerative braking, automatic control of the braking forces on front and rear wheels, and wheels antilock function together. The front-rear torque is allocated exploiting the maximum longitudinal force transmissible, and the electric motors provide the torque until the limit is reached leaving to the friction brakes the role to provide the remaining amount of torque required. Similarly, authors of [20] develop a brake system for an automatic transmission based HEV, which is handled by a regenerative braking cooperative control algorithm that exploits the available motor torque characteristic. Gang and Zhi [21] propose an energy saving control strategy based on motor efficiency map for electric vehicles with four-wheel independently driven in-wheel motors. The four-wheel drive torque is online optimized in real time through drive energy saving control, to improve the driving efficiency in the driving process of electric vehicles. [22] proposes a regenerative braking distribution strategy based on multi-input fuzzy control logic while considering the battery SOC, the brake strength, and the motor speed.

All the above-mentioned approaches focus on a single aspect of the braking maneuver: ideal braking repartition, motor efficiency. The obtained solutions based on optimal control theory must be evaluated minimizing the cost functional on a prefixed drive cycle; on the other hand, an online problem evaluation requires big computational effort. Reported papers concentrate on pure braking maneuvers, in which longitudinal load transfer is considered. However, the lateral load transfer in cornering is not considered. Also yawing moment request by TV stability control is not considered. The resulting algorithms are thus not considering the vehicle lateral dynamics and the influence of the braking torque on the car lateral stability. [23] proposes an optimized control strategy for IWM vehicle, which considers vehicle lateral stability. [24] proposes an optimal control distribution strategy for IWM vehicle considering energy efficiency. However, both strategies are intended for EMs only and do not consider blended braking condition.

In this paper, the proposed strategy distributes the required braking force among four DEMS and the four hydraulic brakes maximizing the recovered energy. Torque distribution accounts for the total braking torque demanded by the driver and the yaw moment required by TV stability control. Furthermore, the distribution algorithm accounts for the wheels applicable torque, because friction is limited by the normal load. Both longitudinal and lateral load transfer are considered to evaluate the wheel condition.

The control strategy optimization problem is solved offline by generating several lookup tables accounting for several vehicle conditions both in straight and in cornering condition.

The paper is thus focused on the optimization of the torque distribution among electric motors and friction brakes, and it is organized as follows. Firstly, the simulation environment is presented accounting for complete vehicle model, driver model, and torque vectoring strategy. Then, an optimal distribution control strategy is presented with details on the design variable and constraints. Some tabulated results of the offline optimization are presented. Finally, the paper shows the simulation results in typical driving maneuvers, where the proposed controller is compared to two other strategies normally adopted in commercial cars.

2. Simulation Environment

To test the performances of the new braking control algorithm, a vehicle model developed in a simulation environment in Matlab/Simulink is used. The vehicle is modelled according to a 14 d.o.f. model (ViCar Realtime), which is based on D segment passengers' car. The model accounts for the following:

(i) Three displacements of the vehicle center of mass (c.o.m);

(ii) Three rotations of the car body (yaw, pitch and roll);

(iii) Four vertical displacements of unsprung masses;

(iv) Four wheels angular velocities about hub axis.

Some subsystems have been added to the ViCar model such as the electric motors model, the friction brake model, driver model, and the TV control logic. All the parameters of the vehicle such as masses, inertias, motors dimension, and brakes dimensions have been designed considering commercial electric vehicles whose main data are reported in Table 1.

2.1. Electric Motor Model. The reference vehicle is driven by four in-wheel motors, which are modelled from a mechanical point of view. The torque versus speed characteristic for both driving and braking is considered as shown in Figure 2. An equivalent first-order time lag transfer function with the same bandwidth of real motors reproduces the dynamics of the motor torque regulator [25]

$$\overline{T_E} = \frac{1}{\tau_m s + 1} T_E, \tag{1}$$

where s is the Laplace coordinate. T_E is the required torque by the controller, while $\overline{T_E}$ is the effective output torque. τ_m is the time constant of motor plus motor drive. In-wheel motors data are taken from [26]. Dimensions of IWM are suitable for $18''$ wheels, which are supported by the considered vehicle.

2.2. Friction Brake Model. The friction brakes have been modelled from a mechanical point of view. As reported in equation (2), the friction torque provided by mechanical brakes is proportional to the oil pressure inside the brake caliper by a constant of proportionality K_b. The dynamics of the oil pressure at the brake caliper are expressed by a pure time delay T_0 combined with a second order transfer function considering oil pump and circuit dynamics, which in Laplace domain reads

$$\overline{p_{\text{cal}}} = e^{-sT_0} \frac{1}{T_1^2 s^2 + T_2 s + 1} p_{\text{cal}}, \tag{2}$$

where $\overline{p_{\text{cal}}}$ is the pressure at the brake caliper, p_{cal} is the pressure required by the control logic, s is Laplace coordinate, and T_1 and T_2 are the brake system time constants.

2.3. Driver Model. Driver model is needed to run close loop maneuver. It is path follower coupled with a cruise control to follow reference speed [10]. The path follower is a proportional controller based on distance error and heading error (see Figure 3):

$$\delta = \frac{2l}{L^2} d K_{p,d} W_d + h K_{p,h} W_h. \tag{3}$$

The first part of the equation refers to distance error; and, the second part refers to heading error. $K_{p,d}$ and W_d are, respectively, the proportional gain and the weight related to the distance error $(d = \cos\psi[Y_{\text{ref}} - (Y_G + L\sin\psi)] - \sin\psi[X_{\text{ref}} - (X_G + L\cos\psi)])$. h is the heading error, and $K_{p,h}$ and W_h are the proportional gain and the weight related to the heading error $(h = \psi_{\text{ref}} - \psi)$. L is the forward preview distance that reproduces driver capability in anticipating its inputs according to road shape in front of the car.

Table 1: Main vehicle parameters.

Symbol	Parameter	Value	Unit
m	Vehicle mass	1947	kg
J_z	Yaw moment of inertia	2559.8	kg m^2
l	Wheelbase	2.875	m
l_f	Com to front axle distance	1.380	m
l_r	Com to rear axle distance	1.495	m
h_G	Com height from ground	0.660	m
c_f	Front track width	1.497	m
c_r	Rear track width	1.495	m

2.4. TV Control Logic. Torque vectoring control strategy is taken from literature ([27]) not being the focus of the present paper. It generates a yaw moment $M_{Z,\text{req}}$ that stabilizes the vehicle and improves its performances by tracking yaw rate and sideslip angle references. It is based on a proportional controller on the vehicle yaw rate $\dot{\psi}$ and vehicle sideslip angle β:

$$M_{Z,\text{req}} = K_{p,\dot{\psi}}(\dot{\psi}_{\text{ref}} - \dot{\psi}) + K_{p,\beta}(\beta_{\text{ref}} - \beta), \tag{4}$$

$K_{p,\beta}$ and $K_{p,\dot{\psi}}$ are the proportional gain on yaw moment and vehicle sideslip angle, respectively. Referring to Figure 3, the reference value of $\dot{\psi}_{\text{ref}}$ and β_{ref} can be calculated from the single-track model as

$$\begin{cases} \dot{\psi}_{\text{ref}} = \dfrac{V\delta}{L\left(1 + K_{U,\text{ref}} V^2\right)}, \\ \beta_{\text{ref}} = \dot{\psi}_{\text{ref}} \left(\dfrac{l_R}{V} - \dfrac{m l_F}{L K_{T,R}}\right), \end{cases} \tag{5}$$

where $K_{U,\text{ref}} = (m/l^2)((l_R/K_{T,F}) - (l_F/K_{T,R}))$ is the desired understeer coefficient.

3. Torque Distribution Algorithm

3.1. Preliminary Considerations. Through the advantages of having four independently wheels driven vehicle, there is the possibility to control independently the torque at each wheel. This powertrain layout leads the possibility to have a nonsymmetric torque distribution around the vehicle allowing torque vectoring. Depending on the driving situation, it is possible to have different performance objectives; in case of panic braking, for example, the driver requires the vehicle to stop in the smallest space possible without losing the vehicle stability and maneuverability. In a commercial passenger car, in normal driving conditions (not panic braking, so for deceleration rates below 6 m/s^2 on dry asphalt), the main objective during braking phase is to recover

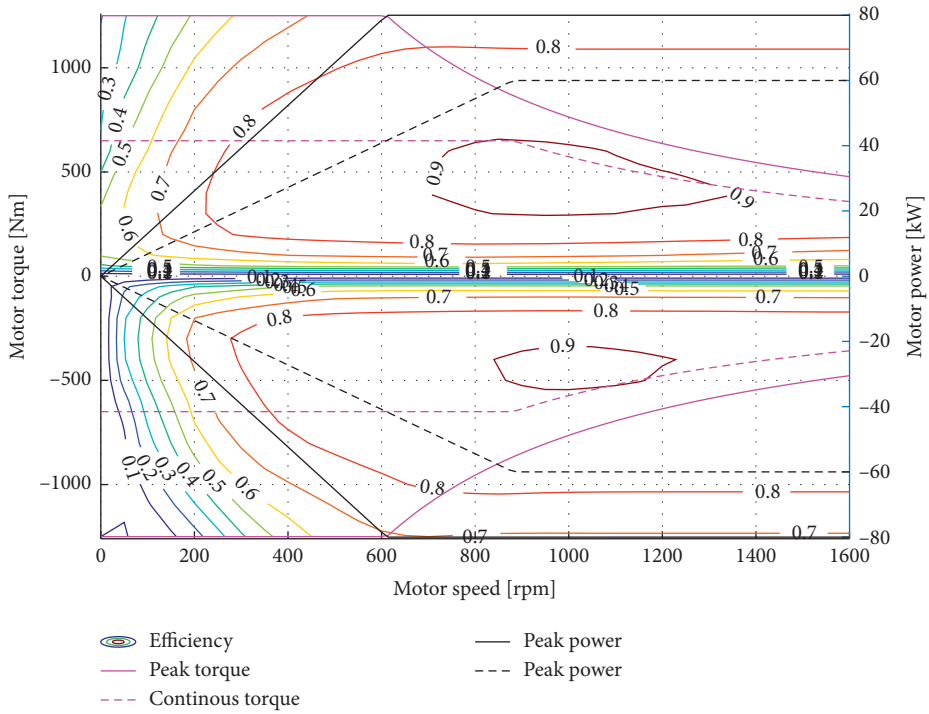

Figure 2: IWM motor curve characteristic. The motor curve characteristic refers to ProteanDrive Pd18 in wheel motor by Protean Electric. The maximum torque of the motor is function of the motor angular speed.

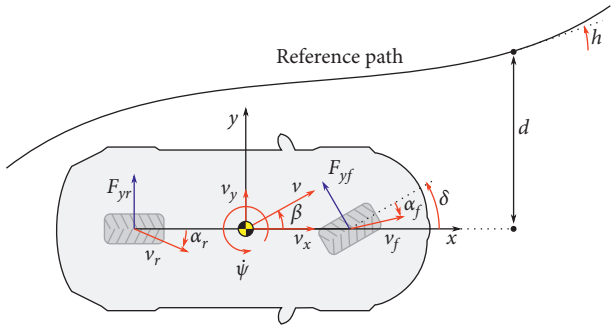

Figure 3: Vehicle single-track model. The TV model used in these simulations is based on the vehicle single-track model.

the vehicle kinetic energy as much as possible guaranteeing anyway the driver requests in terms of longitudinal deceleration and having the possibility to control independently the torque on the left and right side of the vehicle, the yaw moment required by the TV control logic. Having the possibility to provide the braking torque at each wheel exploiting the friction brake and the DEM, the torque distribution problem has been solved with a mathematical optimum-search approach. The problem design variables are eight and correspond to the four friction torques and the four electric torques (i.e., one at each wheel), the objective function considers the DEMs efficiency map and corresponds to the regenerated power for each dynamic condition, and the additional optimum problem constraints consider the vehicle dynamics, driver requirements, and physical limits of the vehicle components.

Figure 4 shows the braking algorithm functional block scheme. The brake pedal position generates a total braking torque request for the controller. The required torque is translated in a brake input considering the possibility of using the electric motors and mechanical brakes based on vehicle dynamics and vehicle energy storage system status. In case of panic braking or low wheel-road friction coefficient, a wheel can lock causing vehicle instability and/or loss of steerability. To avoid wheel locking, the torque at this wheel can be controlled differently, not considering as primary goal the energy regeneration, but the passengers safety. So, at any request of braking torque by the driver, if a wheel is slipping, the torque at that wheel can be controlled using an antilock braking algorithm [3].

Figure 5 represents the scheme of vehicle power flux. During braking maneuver (red arrows), the kinetic energy of the vehicle is transformed by electric motors in electric energy that is delivered to battery storage system. During accelerating maneuvers (green arrows), the energy stored in the battery is delivered to the wheels, passing through inverters, and then it is transformed in kinetic energy. Considering that electric motors and the energy storage system are usually designed for vehicle traction phase, the most critical condition occurs during braking maneuver, where required acceleration performances are higher in traction condition for safety reason. The power to be dissipated when braking is in general much larger than the one required in driving. The battery capacity rate (C_{rate}) and the State of Charge (SOC) are two important parameters to define the battery capability in accepting the input power when regenerative braking is considered. Yaici et al. [28] review different recent application of various battery/supercapacitor

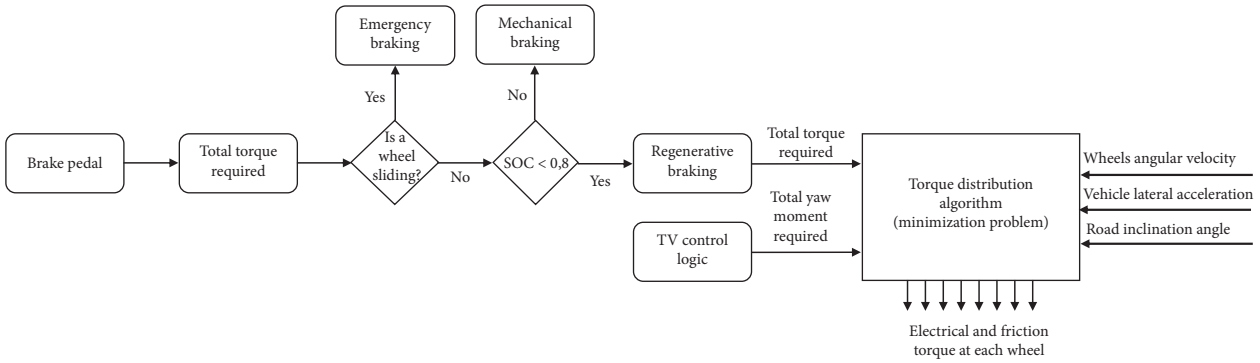

Figure 4: Braking algorithm scheme. The torque distribution algorithm is represented with a black box scheme to underline the algorithm working conditions and the logics inputs and outputs.

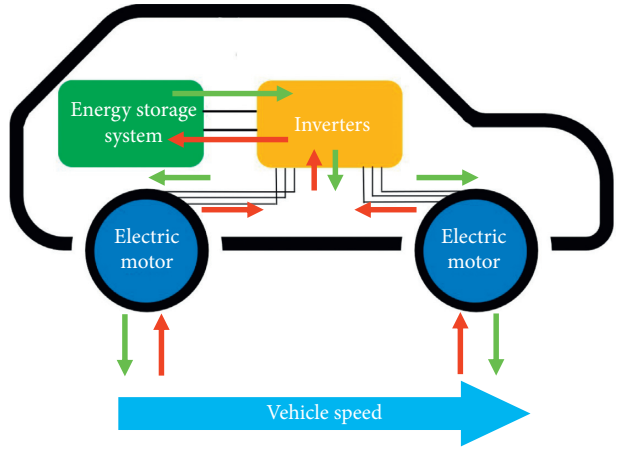

Figure 5: Vehicle power fluxes. The green arrows represent the power fluxes from the batteries to the road during traction phase, and the red arrows represent the power fluxes during regenerative braking.

hybrid system in EVs, and different lithium-ion battery models for automotive applications have been largely treated in literature ([29–31]). From these papers, thanks to the use of the supercapacitors and the presence of different energy storage systems layouts, the problem related to the power flux and the C_{rate} seems to be overcome because the energy storage systems can absorb extremely big amount of power (with respect to HEV/PHEV). The bottleneck of the power in regeneration strategies is now the DEMs. These considerations allow to neglect the impact of the power supply on the braking control algorithm and to consider only motor characteristic and efficiency to impact on the torque distribution optimization.

3.2. Design Variables. The goal of a regenerative braking distribution is to find the correct torque quantity that must be provided from each electric motor and from each brake caliper. So, the problem design variables are the electric and friction torques at each wheel:

$$T_{i,j}, \quad \text{where: } i = \{E, F\} \text{ and } j = \{FR, FL, RR, RL\}. \tag{6}$$

(i) E: electric
(ii) F: friction
(iii) FR: front right wheel
(iv) FL: front left wheel
(v) RR: rear right wheel
(vi) RL: rear left wheel

Thus, the total number of considered design variables is eight: the four electric torques by DEMS and the four friction torques by hydraulic brakes.

3.3. Objective Function. The goal of the optimization problem is to maximize the power recovered during braking maneuver. The power recovered is equal to the braking torque applied at each wheel ($T_{E,j}$) multiplied by the wheel angular speed (ω_j) and the motor efficiency ($\eta(T_{E,j}, \omega_j)$) that, again, is function of the torque required and wheel angular speed. The power that each electric motor can regenerate can be calculated as $P_j = T_{E,j} \cdot \omega_j \cdot \eta(T_{E,j}, \omega_j)$. The torque applied during braking is negative for convention, while the wheel angular speed and motor efficiency are always positive. The total energy recovered during braking maneuver is equal to the sum of the power coming from each wheel. Maximizing the power recovered at each time instant corresponds to maximize the total energy regenerated during the entire period of the braking maneuver. The maximization problem is converted as minimization

problem due to the negative sign of the total power. The objective function can be stated as

$$\min\left[\sum_{j=FR,FL,RR,RL} T_{E,j}\cdot\omega_j\cdot\eta\left(T_{E,j},\omega_j\right)\right]. \tag{7}$$

3.4. Design Variable Space. The design variables space can be described considering the friction brake system, the EMs architecture, and the maximum torque that can be transmitted to the road. The friction brake torque is proportional to the pressure times a constant gain (K_b) as

$$T_F = -K_b p_{\text{cal}}. \tag{8}$$

The minimum values that the friction torque can assume are given by the maximum pressure ($p_{\max}$) that can be reached inside the caliper. The upper bound to T_F is 0 being friction torques always dissipative, and the friction torques domain is thus

$$T_{F,j}\in\left[-K_b p_{\max};0\right],\quad \text{where: } j=\{FR,FL,RR,RL\}. \tag{9}$$

Electric motors can provide negative (regenerative) torque, which is function of motor speed as represented in Figure 2 by solid lines in magenta color. The motor curve characteristic is function of motor peak torque and peak power. For extremely low speed, the EMs can provide negative braking torque but with almost no efficiency. In fact, the efficiency drops below 10% for high braking torques and speeds lower than 150 rpms.

Since the distribution algorithm focuses on braking maneuver, the upper limit of the motor torque is set to zero. The limitations of the electric torques can be expressed as

$$T_{E,j}\in\left[T_{E\min}\left(\omega_j\right);0\right],\quad \text{where: } j=\{FR,FL,RR,RL\}. \tag{10}$$

3.5. Equality Constraints. The equality constraints represent the requirements that must be satisfied. When the car is running, it is necessary that the driver inputs must be respected; thus, the total required torque T_{Req} has to be correctly applied to the car by the torque distributor

$$T_{\text{Req}} = \sum_{j=FR,FL,RR,RL} T_{E,j} + T_{F,j}. \tag{11}$$

Having four independently driven wheels, it is possible to have some torque vectoring on the vehicle, and the optimal asymmetrical torque distribution on the wheels can be computed including the equation (12) to the optimal control problem. $M_{Z,\text{Req}}$ corresponds to the total torque that must be provided to the vehicle and the right part of the equation contains the design variables ensuring that the total yaw moment required can be provided.

$$M_{Z,\text{Req}} = \left(\left(T_{E,FL}+T_{F,FL}\right)-\left(T_{E,FR}+T_{F,FR}\right)\right)\frac{c_F}{2R_w}+\left(\left(T_{E,FL}+T_{F,FL}\right)-\left(T_{E,FR}+T_{F,FR}\right)\right)\frac{c_R}{2R_w}. \tag{12}$$

3.6. Inequality Constraints. The optimal control problem is completed including some additional constraints that must be respected. They are not so binding as the equality constraints because we define a range of values in which the optimal control problem solution must be included. They are necessary to guarantee the vehicle stability during braking maneuver.

Brakes pressure and motor characteristics are not the only limitation when considering wheel dynamics: tire-road adhesion must be considered. The limit force that can be transmitted to the ground is proportional to the vertical load (F_z) acting on the wheel and wheel-road friction coefficient μ. The total torque on the wheel, which is the sum of electric and hydraulic brakes torques, shall not exceed the limit friction torque as expressed in

$$\left|T_{E,j}+T_{F,j}\right|\le\mu F_{Z,j}R_w,\quad \text{where: } j=\{FR,FL,RR,RL\}. \tag{13}$$

To correctly use equation (13), the vertical load at each wheel must be evaluated. This is done by estimating it according to the lateral acceleration, and the wheels angular velocities are normally measured on commercial cars.

The vertical forces at each wheel are computed according to the following equations:

$$\begin{aligned}
F_{z,FR} &= \frac{mg}{2}\left(\frac{l_R}{l}-\frac{A_{x\text{Req}}h_G}{gl}-\frac{2h_G A_y}{c_F g}\left(\frac{K_{\rho F}}{K_{\rho F}+K_{\rho R}}\right)\right),\\
F_{z,FL} &= \frac{mg}{2}\left(\frac{l_R}{l}-\frac{A_{x\text{Req}}h_G}{gl}+\frac{2h_G A_y}{c_F g}\left(\frac{K_{\rho F}}{K_{\rho F}+K_{\rho R}}\right)\right),\\
F_{z,RR} &= \frac{mg}{2}\left(\frac{l_F}{l}+\frac{A_{x\text{Req}}h_G}{gl}-\frac{2h_G A_y}{c_R g}\left(\frac{K_{\rho R}}{K_{\rho F}+K_{\rho R}}\right)\right),\\
F_{z,RL} &= \frac{mg}{2}\left(\frac{l_F}{l}+\frac{A_{x\text{Req}}h_G}{gl}+\frac{2h_G A_y}{c_R g}\left(\frac{K_{\rho R}}{K_{\rho F}+K_{\rho R}}\right)\right).
\end{aligned} \tag{14}$$

With

(i) $A_{x\text{Req}}$: driver required vehicle longitudinal acceleration;

(ii) A_y: vehicle lateral acceleration;

(iii) c_F: vehicle front track;

(iv) c_R: vehicle rear track;

(v) F_z: contact forces perpendicular to the ground;

(vi) g: gravitational acceleration;

(vii) h_G: distance between the center of mass and the ground;

(viii) $K_{\rho F}$: front axle equivalent rolling stiffness

(ix) $K_{\rho R}$: rear axle equivalent rolling stiffness

(x) l: vehicle wheelbase;

(xi) l_F: distance between the center of mass and the vehicle front axle;

(xii) l_R: distance between the center of mass and the vehicle rear axle;

(xiii) m: vehicle mass.

To account for longitudinal load transfer due to longitudinal acceleration, the required driver acceleration ($A_{x\mathrm{Req}}$) is used instead of the measured longitudinal acceleration. This is to avoid undesired chattering in the controller. The desired longitudinal acceleration ($A_{x\mathrm{Req}}$) is calculated as the minimum between the acceleration produced by wheel torques and the friction limit acceleration as

$$A_{x\mathrm{Req}} = \min\left[A_{xT}, A_{x\mu}\right], \tag{15}$$

where A_{xT} is the acceleration produced by total required torque by driver T_{Req}, which is supposed to be applied on the wheel being a hard constraint, and it is computed from the equilibrium of the forces that acts on the vehicle in longitudinal direction. In this way, the longitudinal acceleration is function of the vehicle speed and the driver required torque, allowing to predict the future state of the vehicle instead to measure the actual one.

$$A_{xT} = \frac{1}{m}\left(\frac{T_{\mathrm{Req}}}{R_w} - F_{\mathrm{res}}\right), \tag{16}$$

where F_{res} considers rolling and aerodynamic resistance forces acting on the car.

The friction limited longitudinal acceleration $A_{x\mu}$ depends upon the friction coefficient and the lateral acceleration as

$$A_{x\mu} = -\sqrt{(\mu g)^2 - A_y^2}. \tag{17}$$

This equation considers that the car has a maximum total acceleration given by friction ellipse (μg), when cornering the maximum exploitable longitudinal acceleration is less due to the coupling effect with lateral acceleration A_y.

Other constraints are derived from the European regulation ECE-R13 [32] and define the upper and lower limits of the force distribution on the rear axle with respect the front one (Figure 6(b)), necessary to guarantee vehicle stability during braking maneuver. Looking at the Figure 6(a), from the force equilibrium in longitudinal direction, and considering the limit adhesion conditions, it is possible to write the following equation:

$$F_{xF} + F_{xR} = ma_x = m\mu g, \tag{18}$$

where the same friction coefficient μ is assumed for front and rear wheels.

From equilibrium equations, it is possible to derive the relationship between the front axle contact forces and rear axle contact forces:

$$\frac{F_{xF}}{F_{xR}} = \frac{l_R + \mu h_G}{l_F - \mu h_G}. \tag{19}$$

Combining equations (18) and (19) and eliminating the dependency by the wheel-road friction coefficient (μ), the rear axle force (F_{xR}), in limit conditions, can be expressed as function of front axle force (F_{xF}) as in equation (20). This front-rear axle force distribution is also called ideal distribution.

$$F_{xR} = \left(mg\frac{l_R}{2h_G} - F_{xF}\right) - \frac{mg}{2h_G}\sqrt{l_R^2 - \left(4lh_G F_{xF}\right)}. \tag{20}$$

Equation (13) describes the upper limit of the force transmitted to the rear axle as function of the force that can be transmitted to the front axle (blue line in Figure 6(a)) to avoid rear wheel locking condition, which will result in unstable vehicle behavior. Then, considering the longitudinal contact force at each wheel equal to the sum of electric and friction torque divided by the wheel rolling radius the relative inequality constraint is

$$\frac{T_{E,RR} + T_{F,RR} + T_{E,RL} + T_{F,RL}}{R_w} \le \left(mg\frac{l_R}{2h_G} - \frac{T_{E,FR} + T_{F,FR} + T_{E,FL} + T_{F,FL}}{R_w}\right) - \frac{mg}{2h_G}\sqrt{l_R^2 - \left(4lh_G\frac{T_{E,FR} + T_{F,FR} + T_{E,FL} + T_{F,FL}}{mgR_w}\right)}. \tag{21}$$

The lower limit of the torque at the rear axle with respect to the front one is expressed in the ECE-R13 regulations ([17, 33]) as

$$\frac{a_x}{g} \ge 0.1 + 0.85\,(\mu - 0.2). \tag{22}$$

Making the same substitutions done for the upper limitations, the lower limit on torque distribution can be expressed as

$$\left|\frac{\sum_{j=FR,FL,RR,RL} T_{E,j} + T_{F,j}}{R_w}\right| \ge 0.1 + 0.85\,(\mu - 0.2). \tag{23}$$

Finally, an inequality constraint is necessary to avoid situations, in which the front and rear yaw moment have an opposite sign as follows:

$$M_{zF} \cdot M_{zR} \ge 0. \tag{24}$$

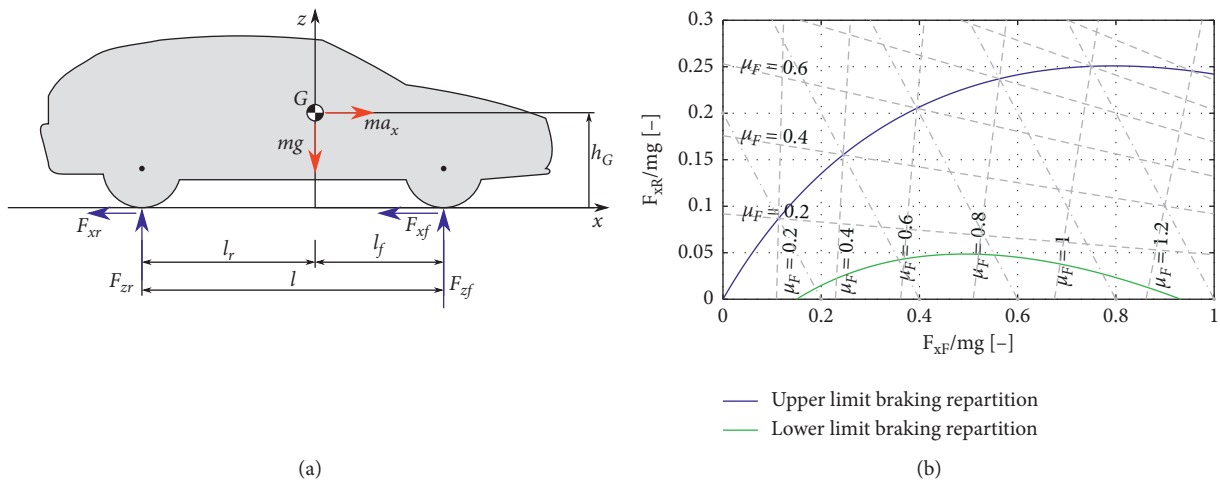

(a) (b)

FIGURE 6: Front right brake distribution limitations. (a) Scheme of vehicle forces when braking. (b) Normalized front-rear force distribution limitations according to ECE-R13 regulation.

3.7. Minimization Problem Numerical Results. The torque minimization algorithm depends on driver inputs, like the driver required torque, stability control system, the total yaw moment required, and car state, the wheel angular velocity, and the lateral acceleration. The solution of such a minimization problem requires a computational effort that would require an expensive solver to be run in real time. The algorithm is thus solved offline considering a range of values of the input parameters and then is implemented on the vehicle with lookup tables that are linearly interpolated. Table 2 reports the considered boundary values of input parameters.

The total torque required by the driver is limited to an absolute value of 4000 Nm because this torque is sufficient to provide the vehicle a deceleration of about 6 m/s^2 on dry asphalt ($\mu = 0.9$), without incurring in wheel locking conditions. Since the torque distribution analyzed refers to a commercial passenger car in normal driving conditions, this value of deceleration is sufficiently high. In addition, the algorithm developed has been solved considering a tire road friction coefficient equal to 0.9, considering that for lower friction coefficients the wheel sliding condition can be avoided thanks to safety systems like the antilock brake system (ABS). The motor speed maximum value is 1600 rpm, which corresponds to a car speed of 200 km/h. The lateral acceleration boundary value is equal to $g = 9.81$ m/s^2 being limited by road adhesion coefficient. Yaw moment range values are derived from motor maximum torque.

The problem has been solved using the Matlab function "*fmincon*," that finds the minimum of constrained nonlinear multivariable functions, applying the "Sqp" method.

Figure 7 represents the solution of the minimization problem in dynamic conditions when vehicle is running on a straight road. When driver requires small braking torque, the vehicle is slowed down by the front axle electric brake only. Instead, when the torque request is higher, the algorithm distributes the braking torque between the front and rear axle according to ideal distribution. This result is due to load transfer that increases the front axle vertical load and allows the front wheels to deliver more braking torque to the ground. Looking at motor efficiency map (Figure 2), it becomes clear why the solver prefers to use higher torques on two motors than smaller torques on four motors. Due to limitations on minimum use of rear axle, a certain torque is requested to the rear axle even if this worsens the total efficiency.

Friction brakes are used to compensate for the lack of electric torque at extremely low motor speed on both axles. In front axles, the friction brakes are also used at higher speed, where the electric motor torque is saturated according to motor characteristics. In the rear axle, on the other hand, the friction brakes are not used at high speed, since the motor torque is enough to brake the wheels. This happens because of load transfer that unloads the rear wheels thus reducing the transferrable longitudinal force. Road adhesion is thus limiting the wheel braking torque and not the motor characteristic.

4. Simulations Results

4.1. Comparing Strategies. To compare the new torque control logic, two alternatives control logics have been implemented in the following logic A and logic B, while the control strategy presented in the previous paragraph will be referred to as strategy C.

Strategy A (blue line in Figure 8) exploits a proportional front-rear brake repartition. This distribution is usually adopted in vehicles with mechanical brake distributor, in which the front to rear repartition is fixed. In this case, the proportionality coefficient is equal to the ratio between the rear and the front brake equivalent coefficients ($K_{b,F}$ and $K_{b,R}$, respectively) until the force at the rear axle does not overcome the limit of ideal force distribution. Then, the torque distribution at the rear axle remains constant for any value of torque required, and only the force at the front axle increases. Transition from linear to constant rear axle torque corresponds to front-rear distribution value when the

Table 2: External parameters discretization for minimization problem.

Variable	Symbol	Min value	Max value	Unit	Points
Driver required torque	T_{req}	−4000	0	Nm	21
Wheel/motor angular velocity	ω_w	0	1600	rpm	21
Yaw moment required	$M_{z,req}$	−1500	1500	Nm	11
Lateral acceleration	A_y	−g	g	m/s^2	11
Road slope	α	−10	10	deg	11

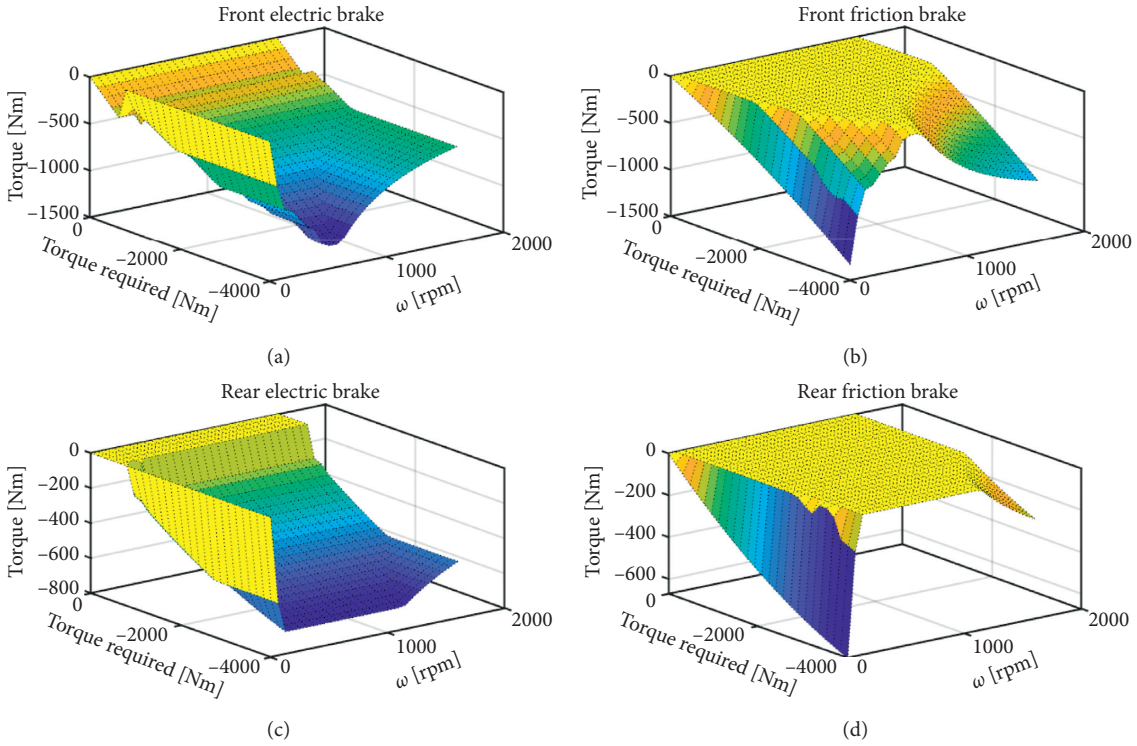

Figure 7: Friction and electric braking torque distribution on the front and rear wheels in dynamics conditions: $M_{z,req} = 0$, $A_y = 0$, and $\alpha = 0$. The results refer only to the front right and rear right wheel because, for the parameters selected, the problem is symmetric.

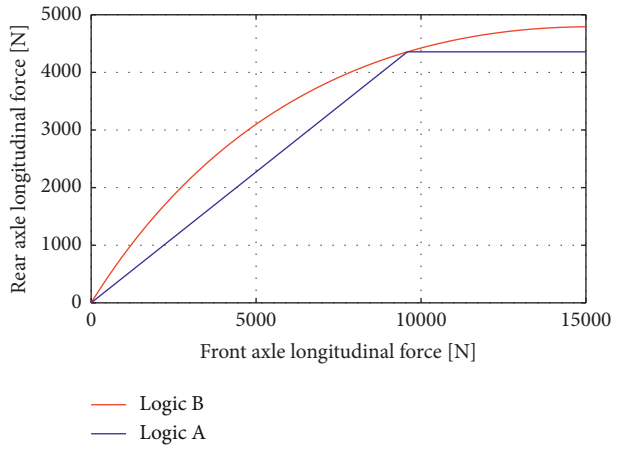

Figure 8: Braking distribution strategies A and B. The blue line refers to distribution strategy A, and the red line to the distribution strategy B that is equivalent to the ideal distribution.

proportional curve intersects the ideal braking distribution (see Figure 8).

Strategy B exploits the ideal front-rear toque distribution (red line in Figure 8). This repartition is the most used in literature ([12, 17–20]) because it guarantees the minimum stopping distance, increasing the braking performances.

For both strategies, the total braking torque required is provided by the braking system exploiting the electric braking torque until the motor limit is reached; then, the remaining demanded torque is provided by friction brakes.

The yaw moment necessary to satisfy the TV request is split front to rear according to the front to rear distribution strategy. Then, each wheel contributes to generating half of the total yaw moment required at the respective axle as

$$\begin{cases} T_{FR} = \dfrac{1}{2}T_F - M_{Z\mathrm{Req}}\dfrac{T_F}{T_{\mathrm{Req}}}\dfrac{R_w}{c_F}, \\ T_{FL} = \dfrac{1}{2}T_F + M_{Z\mathrm{Req}}\dfrac{T_F}{T_{\mathrm{Req}}}\dfrac{R_w}{c_F}, \\ T_{RL} = \dfrac{1}{2}T_R - M_{Z\mathrm{Req}}\dfrac{T_R}{T_{\mathrm{Req}}}\dfrac{R_w}{c_R}, \\ T_{RR} = \dfrac{1}{2}T_R + M_{Z\mathrm{Req}}\dfrac{T_R}{T_{\mathrm{Req}}}\dfrac{R_w}{c_R}, \end{cases} \tag{25}$$

T_F and T_R are the total required torques on front and rear axle, respectively. R_w is the wheel rolling radius, and c_F and c_R are the front and rear track half width.

4.2. Longitudinal Dynamics Simulations Results

4.2.1. Constant Deceleration Braking Maneuvers. To compare the effects of the new control logic (logic C) with A and B, in all the range of required torque, in which it has been designed to operate, a braking maneuver is simulated, in which the initial speed is set to 200 km/h, and then constant deceleration speed profile is requested until the vehicle stops. The maneuvers have been performed in a Matlab/Simulink simulation environment using the vehicle model previously described. The vehicle speed is regulated thanks to a cruise control, which generates the driver demanded braking torque.

Figure 9 shows the power regeneration efficiency during braking maneuver as function of vehicle velocity and vehicle deceleration. The power regeneration efficiency $\eta_{\mathrm{reg}W}$ is computed as

$$\eta_{\mathrm{reg}W} = \frac{W_{\mathrm{reg}}}{m_{\mathrm{eq}}a_x v}, \tag{26}$$

where W_{reg} is the effective power that is regenerated, which is normalized with respect to the inertia forces power, which accounts for equivalent car mass m_{eq} (mass plus rotating inertias).

Logic C regenerates more, or at least equal, power than the other two. More in detail, due to the larger use of the front axle motors (Figures 10 and 11), the power regenerated is higher when the motor torque request is low, i.e., for small deceleration values typical of urban driving scenarios as better shown in following simulations. In fact, looking at motor efficiency map (Figure 2), the efficiency is low at low torque values. For low decelerations, a torque distribution strategy that accounts for motor efficiency can show larger performance improvements. For deceleration greater than 0.2 g, the distribution of the logics B and C is the same, and so also the power regenerated. The difference between the three strategies is in the order of few % points. To better highlight the differences, the following additional considerations are drawn.

Figure 10 shows the electric and friction torques applied, respectively, at the front and the rear vehicle axle with respect to car speed in low-speed range 0–50 km/h. Figure 11 reports same quantities but in high-speed range 50–150 km/h. Since pure straight driving conditions are considered, the left to right torque distribution is even for all the considered control strategies. At lower decelerations (−0.1 g in Figure 10), all the strategies are not using the rear friction brakes, since the EMs are enough to apply the required torque. Looking at the front to rear torque distribution, it is possible to notice that logic A and logic B are distributing the torque front to rear according to defined ratios, while logic C is adopting only front motors to achieve the same car deceleration. This allows to recover more energy, since the total efficiency is higher when two motors are not used (rear ones), while the other two (front ones) are used with higher torque. Front and rear friction brakes are used only by logic C below 10 km/h, where the front electric motor efficiency is close to zero. Logic A and logic B use friction brakes for speeds below 1 km/h.

For middle deceleration (−0.3 g in Figure 10), strategies B and C distribute the torque at the front and rear axle at the same time, and the electromechanical distribution is the same.

At higher deceleration (−0.5 g in Figure 10), on the contrary, strategy B delivers to motors the maximum electric torque that they can exploit, while logic C follows a strategy that favors the best motor efficiency. In this way, the distribution is different, and the energy recovered is slightly higher. At deceleration of 0.5 g and for vehicle speed below 50 km/h, logic C recovers more power with respect logic B, due to better exploitation of the motor efficiency map.

To further analyze the obtained results, the total recovered energy during the braking maneuver is computed. The energy is then divided by the total vehicle kinetic energy at the beginning of the braking maneuver ($E_k = (1/2)m_{\mathrm{eq}}v_0^2$ where v_0 is 200 km/h), which represents the ideal maximum recoverable energy during the whole braking maneuver. This ratio can thus be seen as the energy regeneration efficiency $\eta_{\mathrm{reg}E}$ of the braking maneuver:

$$\eta_{\mathrm{reg}E} = \frac{E_{\mathrm{reg}}}{E_k}. \tag{27}$$

Top graph in Figure 12 shows the results of energy efficiency for the previously presented braking maneuver for several deceleration values. Bottom graph in Figure 12

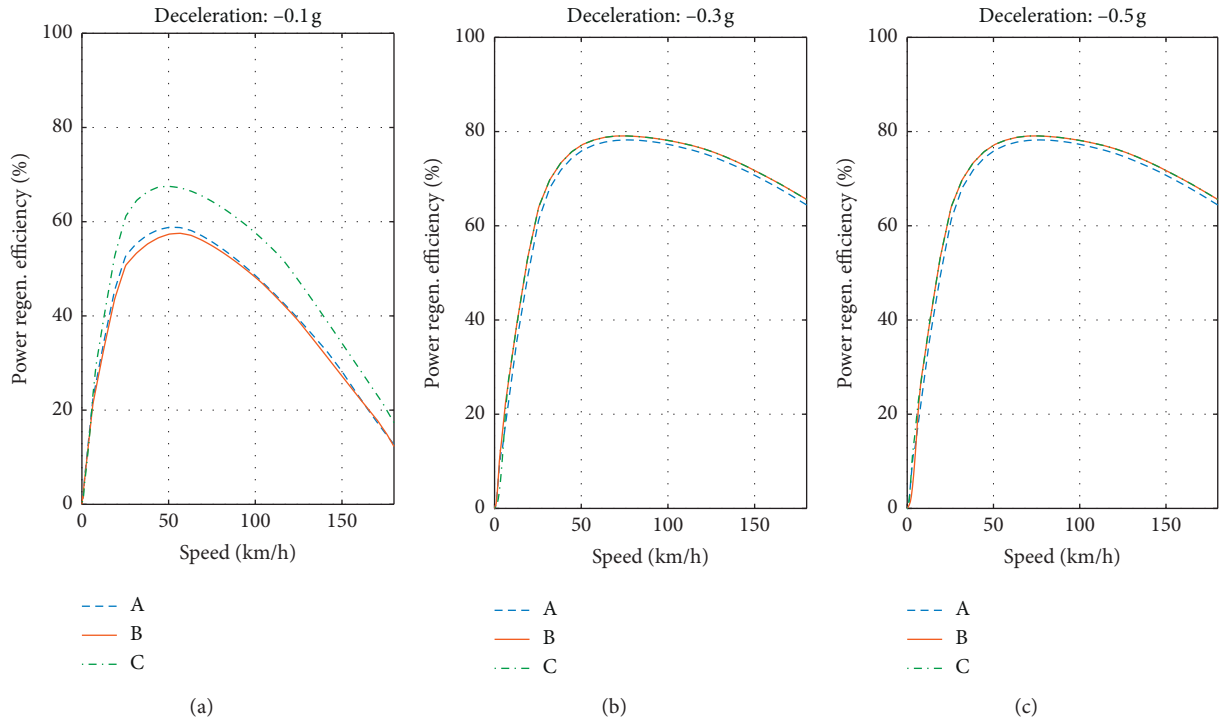

Figure 9: Power regeneration efficiency at different decelerations as function of vehicle speed. Blue line: logic A; red line: logic B; green line: logic C.

represents the relative improvement of logic C with respect to logic A and logic B: $\varepsilon_{C/A}$ and $\varepsilon_{C/B}$. These coefficients are computed as the ratio between the recovered energy of logic C and the one recovered by logic A and logic B, respectively:

$$\varepsilon_{C/A} = \frac{E_{\text{reg}C}}{E_{\text{reg}A}}, \qquad \varepsilon_{C/B} = \frac{E_{\text{reg}C}}{E_{\text{reg}B}}. \tag{28}$$

The results confirm that, for low deceleration, the relative energy saved is higher for strategy C, and that strategy A is better than logic B due to the larger use of the front axle.

Figure 13 reports the longitudinal forces on the vehicle rear axle as function of the front axle ones where it is possible to appreciate the front to rear distribution for the three strategies.

4.2.2. Driving Cycles. To further analyze the controls performance in straight driving, two urban driving cycles, the NEDC [32] and WLTP [10], are simulated. The tests have been performed using the vehicle model described above and using a PI controller on vehicle speed to make the vehicle follow the velocity profile. Since the attention is posed on the braking phase, the driving distribution strategy is the same for the three logics, and its performance is not considered here.

Figure 14 reports the total energy recovered from electric motors in the two driving cycles, highlighting the contribution of each wheel. It is to point out that, in NEDC, the deceleration is always lower than 1 m/s^2, while in urban WLTP cycle it is slightly higher but still small (1.5 m/s^2) if compared to the braking performance of the car on dry asphalt. In such driving condition, a control strategy that considers motor efficiency shows greater benefits. In fact, in both driving scenarios, the energy recovered from strategy C is considerably higher than that of strategies A and B. Table 3 summarizes the results obtained by reporting the total regenerated energy (E_A, E_B, and E_C) and the relative one ($\varepsilon_{C/A}$ and $\varepsilon_{C/B}$ as from equation (28)). Strategy C recovers 19% more than strategy A and 22% more than strategy B in NEDC, while in WLTP strategy C recovers 15% more than strategy A and 17% more than strategy B. This happens because strategy C prefers to brake with only one axle, thus increasing the demanded braking torque, which makes the motors work in a better working range. Figure 15 shows the working range of front and rear wheels for the three strategies. The color of the points in the graph refers to the motor efficiency. Again, it is possible to see how strategy C is preferring to use only front axle to maximize the motor efficiency. This choice shows significant benefits, and logic C shows higher recovered energy in both driving cycles. Comparing the two cycles, due to higher decelerations in the WLTP cycle, the use of the rear wheels is larger in the latter.

4.3. Track Simulations Results. To test the controller performance including the effect of vehicle lateral dynamics, a circuit track has been simulated (Figure 16(a)). The aim of this simulation is to inquire the effect of TV on the

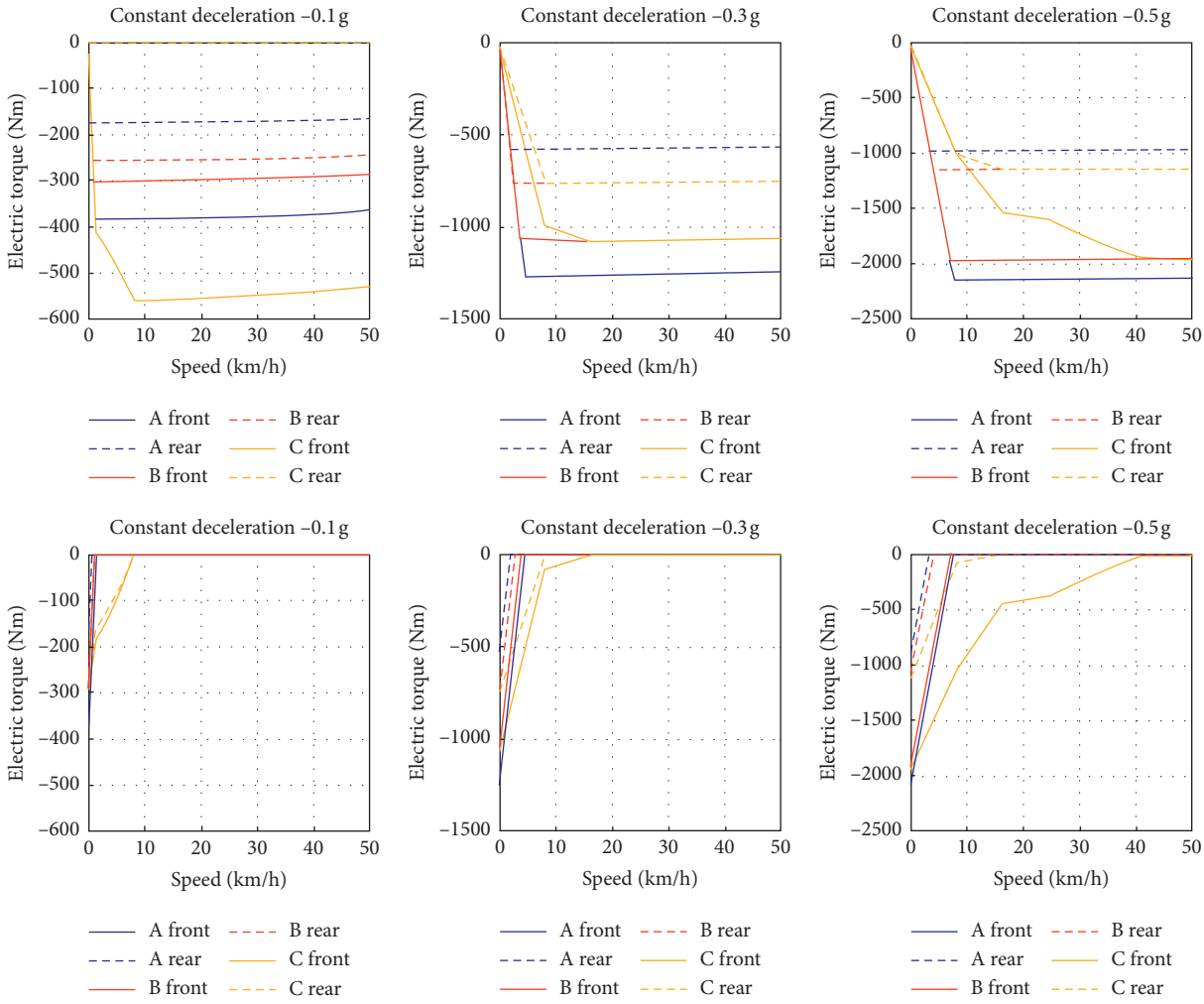

Figure 10: Torque as function of speed during constant deceleration braking maneuvers, comparison of control strategies A, B, and C. Upper plots report electric torques, while bottom plots report friction torques, low speed.

distribution strategy in combined longitudinal and lateral dynamics of the car. The selected reference path is taken from GPS data of a real circuit, in which the speed reference profile is built so to achieve desired values of both longitudinal and lateral accelerations. Two sets of acceleration levels are selected as better specified in the following. The reference speed profile of the circuit is offline calculated considering the circuit curvature (Figure 16(b)) and the maximum acceleration and deceleration that the vehicle must reach during the simulation. Given the reference path, the procedures to compute the reference speed are as follows:

(i) Compute trajectory curvature.

(ii) Compute maximum speed to have desired lateral acceleration value according to trajectory curvature.

(iii) Smooth speed obtained to respect maximum and minimum desired longitudinal acceleration in both driving and braking.

Two sets of accelerations are considered as reported in Table 4. Resulting speed and lateral acceleration profiles are reported in Figures 16(c) and 16(d), respectively. Only a sector is reported for clarification and readability of the diagrams.

Figure 17 reports the energies regenerated by the four wheels during 1 lap of the circuit. With the focus being on the braking control strategy, only the energy recovered when braking is reported. The results can also be expressed in relative terms using again equation (28). Table 5 reports the numerical results of relative regenerated energy during one lap simulation to show logic C improvements with respect to logic A and logic B.

Figure 17 results show that, at low decelerations, the energy recovered is higher for the strategy C due to the larger use of the front axle wheels, and these results are coherent with the ones in pure straight driving condition (Figures 7 and 9). Conversely, at higher decelerations, even if strategy A is using more torque in the front than in the rear axle (see column A of Figure 17(b)), the total recovered energy is smaller, since the motors are saturating, and friction brakes in front are used instead of increasing the electric braking torque in the rear axle. Another important aspect to be highlighted is the fact that, at higher deceleration values, the requested electric torque is in general high, which makes the

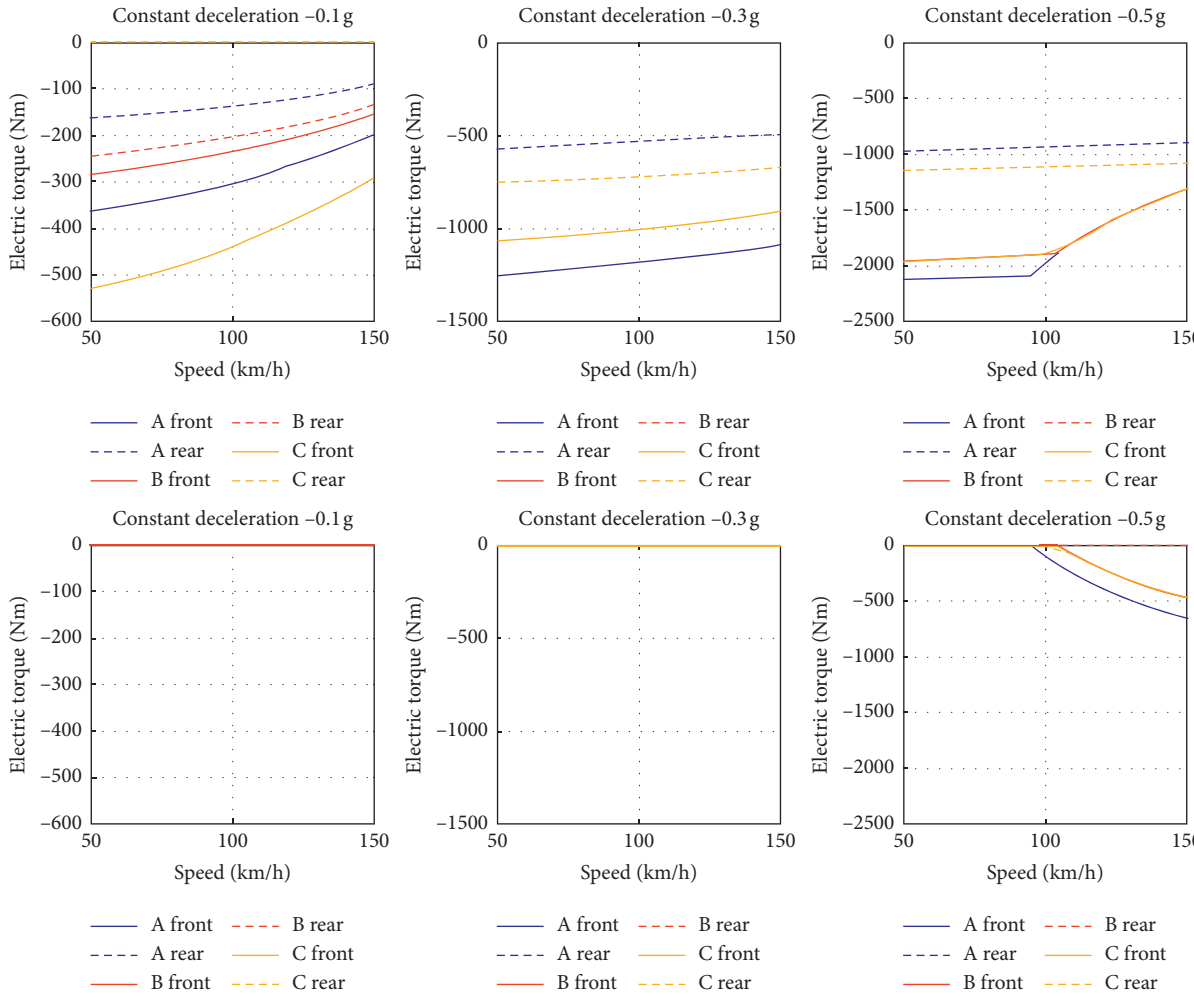

Figure 11: Torque as function of speed during constant deceleration braking maneuvers, comparison of control strategies A, B, and C. Upper plots report electric torques, while bottom plots report friction torques, high speed.

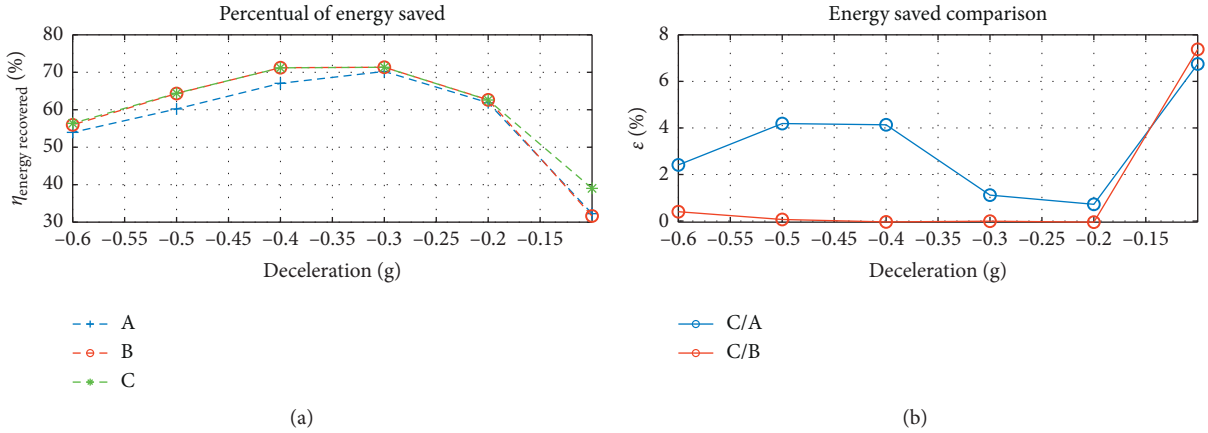

Figure 12: Efficiency of the torque distribution control logics in relative terms during constant deceleration rate braking maneuvers.

electric motors work in a good efficiency point. The benefit of control strategy C is that it is much smaller compared to logics A and B but still positive. Figure 18 shows the working points of the four motors for high-speed profile lap. As already mentioned, the torques required at the motors are large, and then the motors work where the efficiency gradient is smaller, close to the optimum. Due to the performances required at the vehicle, in this situation, all the three logics exploit torque values that are close to the motor limits. In addition, the use of torque vectoring behaves as a hard

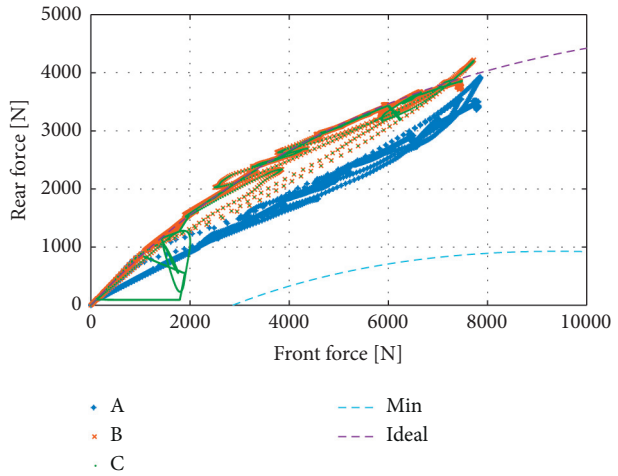

Figure 13: Front rear force distribution between front and rear axle during constant deceleration braking maneuvers.

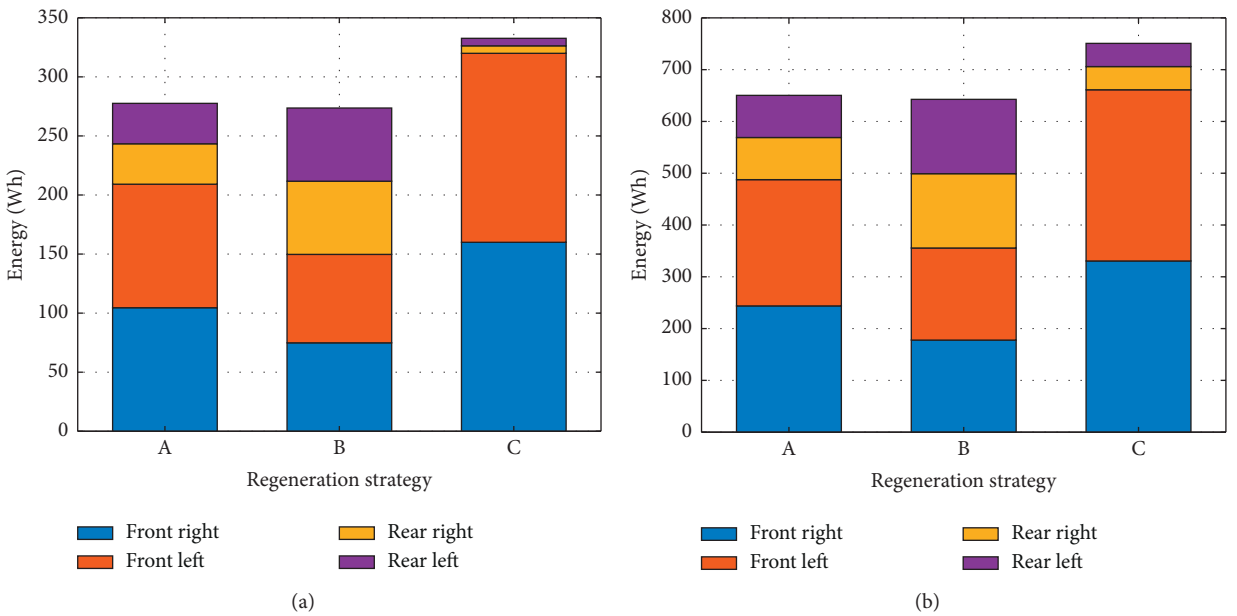

Figure 14: Longitudinal driving cycles energy regenerated for each wheel. (a) NEDC cycle; (b) WLTP cycle.

Table 3: Numerical results of energy regenerated during braking phases in the NEDC and WLTP cycles.

	Symbol	Value	Unit
NEDC	E_A	277.58	Wh
	E_B	273.63	Wh
	E_C	332.64	Wh
	ε_{C-A}	19.83	%
	ε_{C-B}	21.57	%
WLTP	E_A	650.35	Wh
	E_B	642.65	Wh
	E_C	750.76	Wh
	ε_{C-A}	15.44	%
	ε_{C-B}	16.82	%

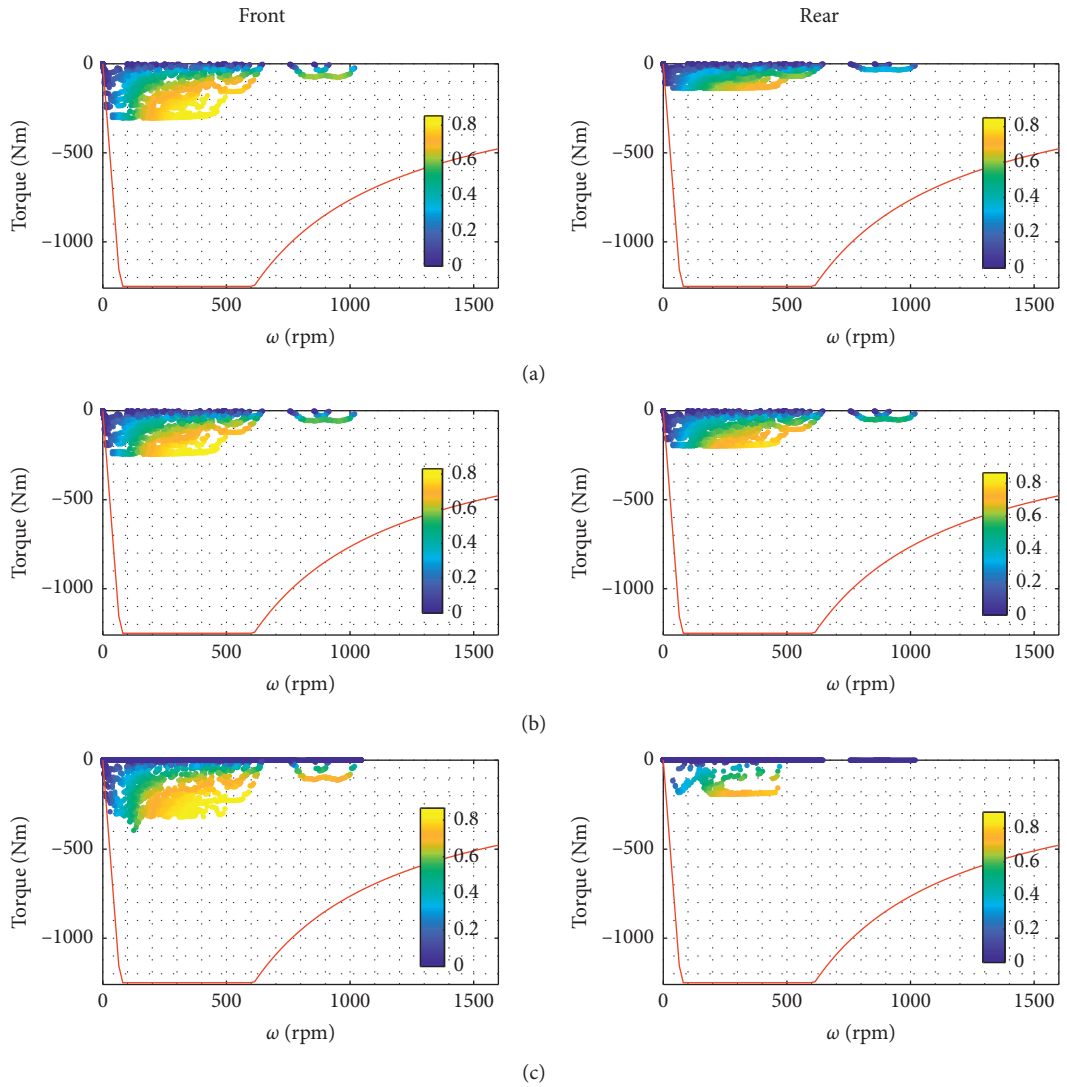

Figure 15: Working range of the front right and rear right motors during the WLTP cycle. In the figures, the efficiency of the motors during the cycle for front and rear wheels and for logic A, B, and C is presented.

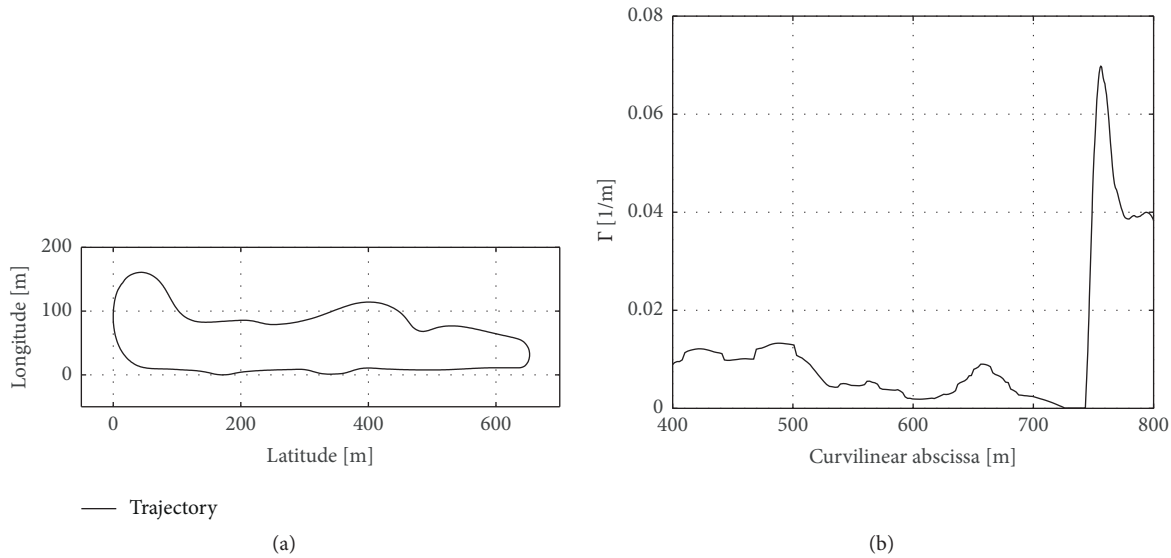

Figure 16: Continued.

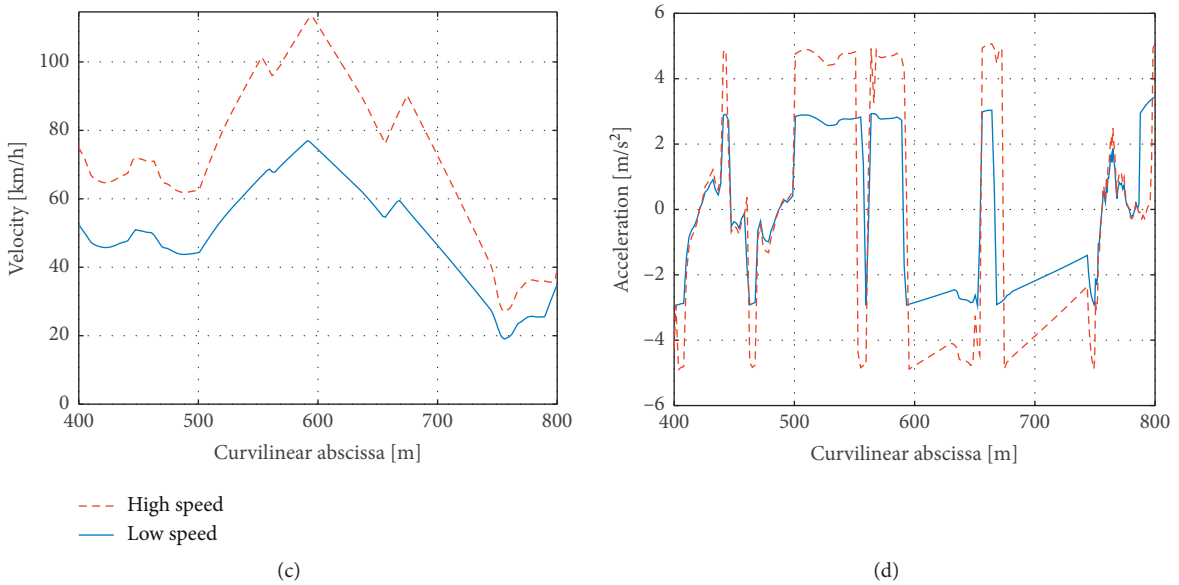

Figure 16: Circuit simulation characteristics. (a) Circuit trajectory. (b) Circuit curvature as function of curvilinear abscissa. (c) Speed profiles as function of curvilinear abscissa. (d) Acceleration profiles as curvilinear abscissa.

Table 4: Acceleration level in track simulation.

	$a_{x,\min}$ (g)	$a_{x,\max}$ (g)	$a_{y,\max}$ (g)
Low speed	−0.2	0.2	0.2
High speed	−0.4	0.4	0.4

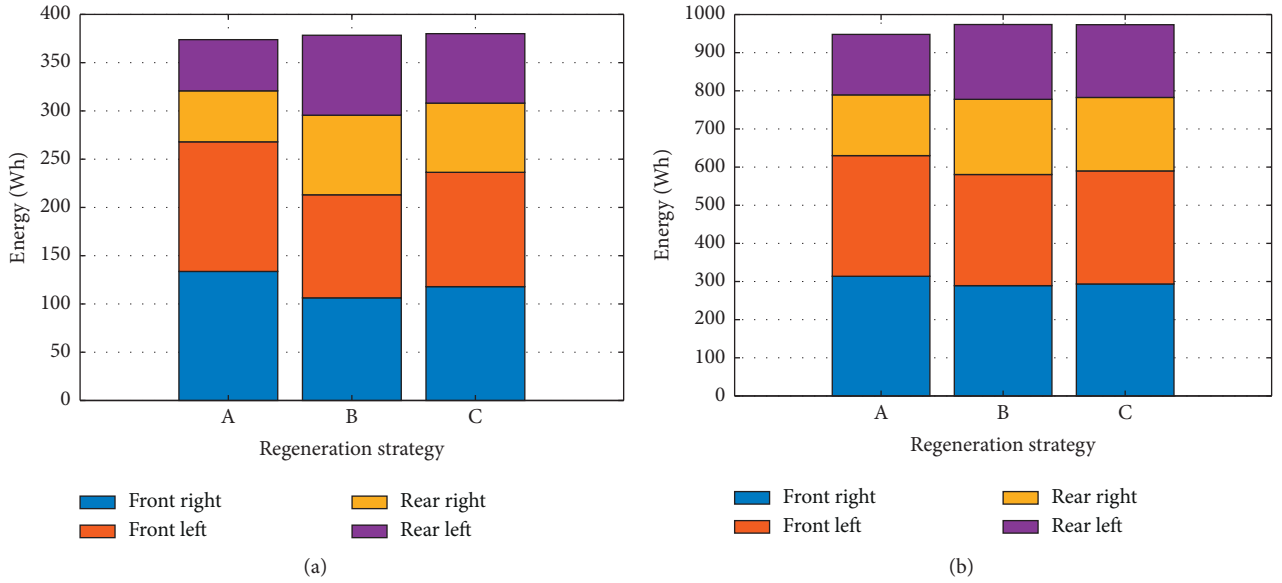

Figure 17: Energy regenerated for each wheel during the lateral dynamic simulations. (a) Low-speed profile. (b) High-speed profile.

Table 5: Numerical results of energy regenerated during braking phases in the lateral dynamics simulations.

	Symbol	Value	Unit
Low-speed profile	ε_{C-A}	2.68	%
	ε_{C-B}	0.43	%
High-speed profile	ε_{C-A}	1.66	%
	ε_{C-B}	0.05	%

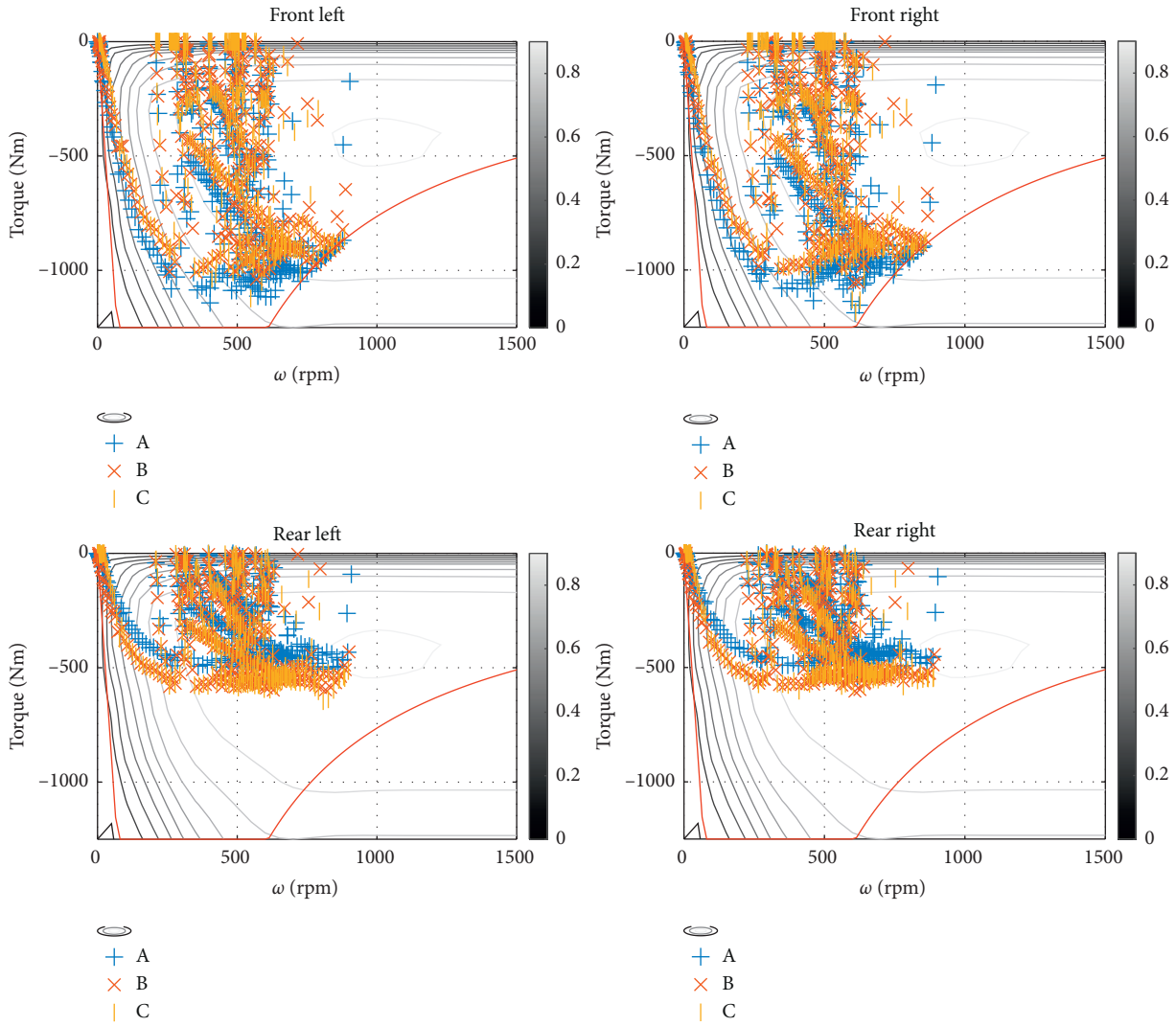

Figure 18: Motors working range during high-speed profile simulation.

constraint in the optimization problem, leading to an extremely limited possibility to increase the performances in terms of energy saved, so the differences in the results are not so evident as the ones seen for pure straight dynamics.

5. Conclusions

The present paper proposes a control strategy that maximizes the regenerated power when braking for vehicles equipped with distributed electric motors, one per each wheel, and conventional friction brakes.

The braking strategy distributes the braking torques among the electric motors and the friction brakes considering the required driver torque and the required yaw moment by torque vectoring stability control system as hard constraints.

The electric motor efficiency and the wheel normal load are used to allocate the torques to maximize the regenerative power under different vehicle conditions of speed, lateral acceleration. Cornering conditions are thus considered; the wheel friction saturation is accounted for considering both longitudinal and lateral load transfers.

Optimization is run offline, and results are stored in lookup tables to be used online. Performance of the proposed controller is compared with other strategies derived from the literature by means of numerical simulations, where typical driving cycles as well as track scenario are considered.

The proposed control shows superior performances in typical urban scenarios, where the vehicle acceleration is small. In fact, the torque allocation, which considers motor efficiency, can gain up to 15% regenerated energy in WLTP driving cycle. Performance is instead comparable, but still higher (1-2%), in more aggressive maneuvers, as the racetrack, where the motor demanded torque is close to the maximum exploitable.

Data Availability

There are no public datasets available. All the information necessary to reproduce results is in the paper.

Conflicts of Interest

The authors declare that they have no conflicts of interest.

References

[1] S. Arrigoni, D. Tarsitano, and F. Cheli, "Comparison between different energy management algorithms for an urban electric bus with hybrid energy storage system based on battery and supercapacitors," *International Journal of Heavy Vehicle Systems*, vol. 23, no. 2, pp. 171–189, 2016.

[2] M. Satoshi, "Innovation by in-wheel-motor drive unit," *Vehicle System Dynamics*, vol. 50, no. 6, pp. 807–830, 2012.

[3] M. Vignati and E. Sabbioni, "Force-based braking control algorithm for vehicles with electric motors," *Vehicle System Dynamics*, vol. 58, no. 9, pp. 1348–1366, 2020.

[4] X. Sun, C. Hu, G. Lei, Z. Yang, Y. Guo, and J. Zhu, "Speed sensorless control of SPMSM drives for EVs with a binary search algorithm-based phase-locked loop," *IEEE Transactions on Vehicular Technology*, vol. 69, no. 5, pp. 4968–4978, 2020.

[5] X. Sun, J. Cao, G. Lei, Y. Guo, and J. Zhu, "A robust deadbeat predictive controller with delay compensation based on composite sliding-mode observer for PMSMs," *IEEE Transactions on Power Electronics*, vol. 36, no. 9, pp. 10742–10752, 2021.

[6] X. Sun, C. Hu, G. Lei, Y. Guo, and J. Zhu, "State feedback control for a PM hub motor based on gray Wolf optimization algorithm," *IEEE Transactions on Power Electronics*, vol. 35, no. 1, pp. 1136–1146, 2020.

[7] M. L. Bacci, F. L. Mapelli, S. Mossina, D. Tarsitano, and M. Vignati, "Wide-speed range sensorless control of an IPM motor for multi-purpose applications," *Inventions*, vol. 5, no. 3, 2020.

[8] F. Braghin, E. Sabbioni, G. Sironi, and M. Vignati, "A feedback control strategy for torque-vectoring of IWM vehicles," *Proceedings of the ASME Design Engineering Technical Conference*, vol. 3, 2014.

[9] G. Park, K. Han, K. Nam, H. Kim, and S. B. Choi, "Torque vectoring algorithm of electronic-four-wheel drive vehicles for enhancement of cornering performance," *IEEE Transactions on Vehicular Technology*, vol. 69, no. 4, pp. 3668–3679, 2020.

[10] M. Vignati and E. Sabbioni, "A cooperative control strategy for yaw rate and sideslip angle control combining torque vectoring with rear wheel steering," *Vehicle System Dynamics*, 2021.

[11] T. Goggia, A. Sorniotti, L. De Novellis, and A. Ferrara, "Torque-vectoring control in fully electric vehicles via integral sliding modes," in *Proceedings of the American Control Conference*, pp. 3918–3923, Portland, OR, USA, June 2014.

[12] W. Xu, H. Chen, H. Zhao, and B. Ren, "Torque optimization control for electric vehicles with four in-wheel motors equipped with regenerative braking system," *Mechatronics*, vol. 57, pp. 95–108, 2019.

[13] A. Mangia, B. Lenzo, and E. Sabbioni, "An integrated torque-vectoring control framework for electric vehicles featuring multiple handling and energy-efficiency modes selectable by the driver," *Meccanica*, vol. 56, no. 5, pp. 991–1010, 2021.

[14] M. Grandone, N. Naddeo, D. Marra, and G. Rizzo, "Development of a regenerative braking control strategy for hybridized solar vehicle," *IFAC-PapersOnLine*, vol. 49-11, pp. 497–504, 2016.

[15] C. He, G. Wang, Z. Gong, Z. Xing, and D. Xu, "A control algorithm for the novel regenerative-mechanical coupled brake system with by-wire based on multidisciplinary design optimization for an electric vehicle," *Energies*, vol. 11, p. 2322, 2018.

[16] I. Valentin, O. Javier, P. Thomas, B. Frank, S. Dzmitry, and S. Barys, "Electric and friction braking control system for AWD electric vehicles," in *Proceedings of the Special Session "Vehicle Dynamics Control for Fully Electric Vehicles – Outcomes of the European Project E-VECTOORC"*, Maastricht, Netherlands, June 2014.

[17] C. Lv, J. Zhang, Y. Li, and Y. Yuan, "Regenerative braking control algorithm for an electrified vehicle equipped with a by-wire brake system," *SAE Technical Paper 2014-01-1791*, 2014.

[18] Z. Zhou, C. Mi, and G. Zhang, "Integrated control of electromechanical braking and regenerative braking in plug-in hybrid electric vehicles," *International Journal of Vehicle Design*, vol. 58, no. 2–4, 2012.

[19] Y. Gao and M. Ehsani, "Electronic braking system of EV and HEV—Integration of regenerative braking, automatic braking force control and ABS, SAE transactions," *Journal of Passenger Cars: Electronic and Electrical Systems*, vol. 110, pp. 576–582, 2001.

[20] J. Ko, S. Ko, H. Son, B. Yoo, J. Cheon, and H. Kim, "Development of a brake system and regenerative braking cooperative control algorithm for automatic-transmission-based hybrid electric vehicles," *IEEE Transactions on Vehicular Technology*, vol. 64, no. 2, 2015.

[21] L. Gang and Y. Zhi, "Efficiency saving control based on motor efficiency map for electric vehicles with four-wheel independently driven in-wheel motors," *Advances in Mechanical Engineering*, vol. 10, no. 8, pp. 1–18, 2018.

[22] B. Xiao, H. Lu, H. Wang, J. Ruan, and N. Zhang, "Enhanced regenerative braking strategies for electric vehicle dynamic performance and potential analysis," *Energies*, vol. 10, p. 1875, 2017.

[23] X. Zhang, K. Wei, X. Yuan, and Y. Tang, "Optimal torque distribution for the stability improvement of a four-wheel distributed-driven electric vehicle using coordinated control," *Journal of Computational and Nonlinear Dynamics*, vol. 11, no. 5, 2016.

[24] L. Guo, X. Lin, P. Ge, Y. Qiao, L. Xu, and J. Li, "Torque distribution for electric vehicle with four in-wheel motors by considering energy optimization and dynamics performance," in *Proceedings of the IEEE Intelligent Vehicles Symposium*, pp. 1619–1624, Los Angeles, CA, USA, June 2017.

[25] F. L. Mapelli and D. Tarsitano, "New generation of electric vehicles [internet]," Edited by Z. Stevic, Ed., InTech, London, UK, 2012.

[26] Protean: Protean Drive P18, 2020, https://www.proteanelectric.com/technology/#overview.

[27] L. De Novellis, A. Sorniotti, and P. Gruber, "Optimal wheel torque distribution for a four-wheel-drive fully electric vehicle," *SAE International Journal of Passenger Cars - Mechanical Systems*, vol. 6, no. 1, pp. 128–136, 2013.

[28] W. Yaici, L. Kouchachvili, E. Entchev, and M. Longo, "Performance analysis of battery/supercapacitor hybrid energy source for the city electric buses and electric cars," in *Proceedings of the 2020 IEEE International Conference on Environment and Electrical Engineering and 2020 IEEE Industrial and Commercial Power Systems Europe, EEEIC/I and CPS Europe 2020*, Madrid, Spain, June 2020.

[29] S. M. Mousavi and G. M. Nikdel, "Various battery models for various simulation studies and applications," *Renewable and Sustainable Energy Reviews*, vol. 32, pp. 477–485, 2014.

[30] A. Fotouhi, D. J. Auger, K. Propp, S. Longo, and M. Wild, "A review on electric vehicle battery modelling: from lithium-ion

toward lithium-sulphur," *Renewable and Sustainable Energy Reviews*, vol. 56, pp. 1008–1021, 2016.

[31] A. Damiano, C. Musio, and I. Marongiu, "Experimental validation of a dynamic energy model of a battery electric vehicle," in *Proceedings of the 4th International Conference on Renewable Energy Research and applications*, Palermo, Italy, November 2015.

[32] UNECE, "UN regulation No. 154–Worldwide harmonized light vehicles test procedure (WLTP)," 2020, https://unece.org/transport/documents/2021/02/standards/un-regulation-no-154-worldwide-harmonized-light-vehicles-test.

[33] Regulation No 13-H of the Economic Commission for Europe of the United Nations (UN/ECE)—Uniform Provisions Concerning the Approval of Passenger Cars with Regard to Braking [2015/2364].

[34] H. B. Pacejka, "Tyre and vehicle dynamics," 2012.

[35] F. Braghin and E. Sabbioni, "A dynamic tire model for ABS maneuver simulations," *Tire Sci Technol*, vol. 38, no. 2, pp. 137–154, 2010.